Lasers in Manufacturing Conference 2017

Interaction of powder jet and laser beam in blown powder laser deposition processes: Measurement and simulation methods

Florian Wirth[a,*], Sebastian Freihse[b], Daniel Eisenbarth[a] , Konrad Wegener[b]

[a]*inspire AG, ETH Zürich, Technoparkstrasse 1, 8005 Zurich, Switzerland*
[b]*Institute of Machine Tools and Manufacturing, ETH Zürich, Leonhardstrasse 21, 8092, Zurich, Switzerland*

Abstract

The coating process by laser cladding as well as additive manufacturing by direct metal deposition are both influenced by the powder jet characteristics and by the interaction between powder jet and laser beam. This is especially true in the newly developed high-speed laser cladding process where this interaction is of great importance as the melting of the powder particles even before reaching the melt pool is desired. A simulation model is presented, which predicts the characteristics of the powder jet between powder nozzle and working plane and also how influential the powder jet will be on the laser beam in terms of attenuation. A new measurement method has been elaborated to analyze the powder particle density distribution in the working plane under conditions that replicate the actual process. This is in order to characterize the powder jet and validate the simulation results. Moreover, a new measurement method which may reveal the powder particle absorption coefficient is proposed. All this allows for the optimal alignment of the powder jet with the laser beam in high-speed laser cladding as well as general predictions of the laser cladding process results by simulation.

Keywords: Laser cladding; direct metal deposition; laser powder interaction; powder jet characteristics; attenuation

1. Introduction

Laser cladding does not only enable a defensive coating of machine parts against corrosion or wear, but also the additive manufacturing of three-dimensional parts. The latter is often referred to as direct metal deposition (DMD), laser metal deposition (LMD), laser engineered net shaping (LENS), laser additive

* Corresponding author. Tel.: +41 44 633 78 74; fax: +41 44 632 11 59.
E-mail address: wirth@inspire.ethz.ch.

manufacturing (LAM) or direct energy deposition (DED). The principal however remains the same, as shown in Fig. 1. Powder is injected into the melt pool, which is created by the laser beam. Moving the powder nozzle together with the laser beam results in the deposition of a weld track. Several overlapping weld tracks form a coating or one of multiple layers of a three-dimensional part. According to Weisheit et al., 2013 there is an ever increasing potential across multiple fields for the application of this technology.

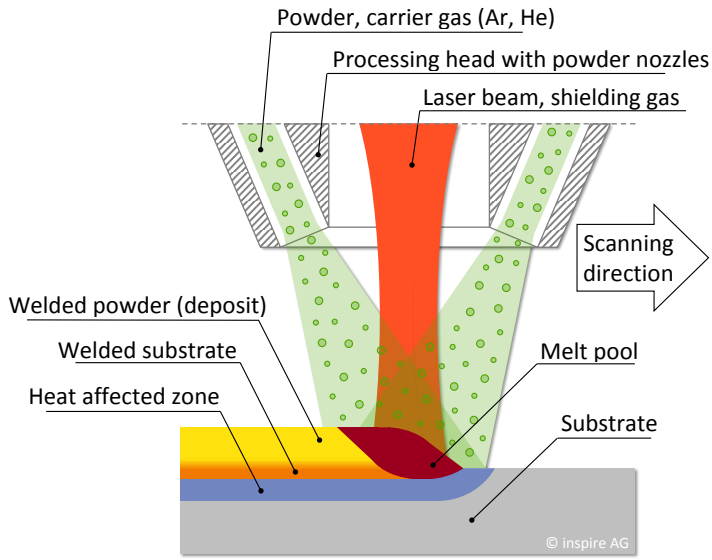

Fig. 1. Principle of the laser cladding process

Furthermore, a modified laser cladding process has been developed in the form of high-speed laser cladding. Schopphoven et al., 2016 show, that this process allows thinner coatings than conventional laser cladding in the range of 10 – 250 µm at higher surface rates of up to 500 cm^2/min and feed speeds of up to 200 m/min with a small dilution zone <5 µm. For this purpose the powder as well as the laser beam must be focused to a diameter below 1 mm, where the powder focus is slightly raised, resulting in the heating of the powder particles up to melting temperature before they reach the melt pool. According to Mueller et al., 2016 the interaction of the laser beam with the flying powder particles and substrate surface is also an essential factor in the deposition of copper circuit traces on polymer or on other materials by laser cladding. Moreover, it has already been shown by Marsden et al., 1992 that for conventional laser cladding, the overall process absorptivity can intensify with a higher powder feed rate. The interaction of the flying powder particles with the laser beam should never be neglected as it can be crucial in processes like high-speed laser cladding. Unfortunately, in situ measurements for process optimization, like that of the powder particle temperature during laser cladding, are hardly possible as they require a high-speed thermographic camera or other costly equipment. What follows is a simulation model which allows the investigation of the processes between powder nozzle and the workpiece surface while generating the necessary input data for melt pool simulation in terms of laser beam attenuation by the flying powder particles. The model is supported by particle velocity measurements as well as by the results of a new powder particle density measurement method. This close attention to measurement differentiates the model from others such as those of Huang et al., 2006, Pinkerton, 2007, Zekovic et al., 2007, Ibarra-Medina et al., 2011, Tabernero et al., 2012, Morville et al., 2012, or Zhang & Coddet, 2016, the first two being analytical and the latter numerical models.

Nomenclature

A_c	carrier gas inlet cross-sectional area
A_s	shield gas inlet cross-sectional area
d_p	particle diameter
$\mathbf{F}$	volume force
$\mathbf{F_{drag}}$	drag force
$\mathbf{F_g}$	gravity force
k	turbulent kinetic energy
m_p	particle mass
m_t	powder particle density distribution
$\mathbf{n}$	normal vector
p	pressure
P_K	Reynolds stress
r	radius
$\mathbf{u}$	fluid velocity
u_c	velocity at the carrier gas and powder inlet
u_s	velocity at the shield gas inlet
$\mathbf{v}$	particle velocity
$\mathbf{v_c}$	initial velocity
$\dot{V}_c$	carrier gas flow
$\dot{V}_s$	shield gas flow
ϵ	turbulent dissipation rate
μ	dynamic viscosity
μ_t	eddy viscosity
ρ	density
ρ_p	particle density
$\mathbf{I}$	unity tensor
C_μ, $C_{\epsilon 1}$, $C_{\epsilon 2}$, σ_k, σ_ϵ	turbulence model parameters
ζ, ζ_1, ζ_2	random number

2. Density measurement and numerical modeling of powder stream

The following measurements were carried out on a CNC laser machine type Trumpf TruLaser Cell 7020 using a three-jet powder nozzle type 3-JET-SO16 by Fraunhofer-ILT with MetcoClad® 625 powder and argon as shield and carrier gas. For the characterization of the powder stream a measurement method was developed, which indicates the powder particle density distribution in the working plane as the amount of powder per area per time that reaches the surface. Here, a plate with a small bore of 0.4 mm in diameter is placed above a balance with a container on it. See Fig. 2 (left). During the measurement the powder nozzle moves over the plate around the bore hole along circular paths starting from the center and traverses after each circulation radially towards the next larger circular path, while the balance continuously measures mass

of powder passing through the bore. The measurement principle is the same as that of Morville et. al, 2012. Although, the measurement is not only carried out in a radial, but also in a circumferential direction, so that the powder stream is characterized in the whole working plane as seen in Fig. 2 (right). Moreover, this method reflects the actual conditions of the laser cladding process when a workpiece in placed below the powder nozzle in contrast with the typical optical measurement method described by Melo, 2015, which requires an unhindered powder jet; as powder particles reflected from the workpiece would affect the measurement.

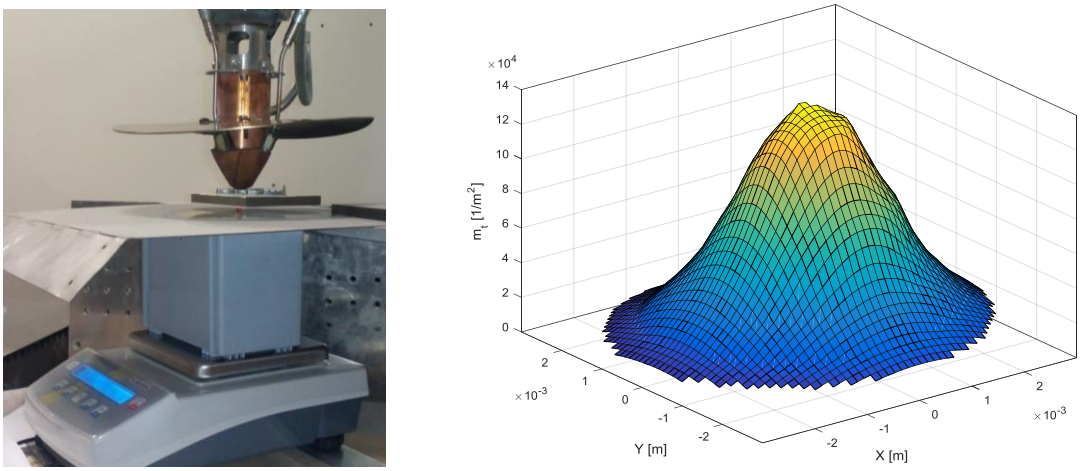

Fig. 2. Powder particle density distribution measurement setup (left) and result (right)

The numerical model of the powder jet was set up using COMSOL Multiphysics 5.2 with its modules “Turbulent Flow, k-ε” and “Particle Tracing for Fluid Flow”. The model geometry shown in Fig. 3 replicates a powder nozzle type 3-JET-SO16 at a working distance of 15 mm comprising a large cylinder, whose bottom represents the substrate surface, while the cylinder sidewall is an open boundary. Three tubes protrude into this cylinder, which constitute the powder channels inside the nozzle. An additional small centric cylinder depicts the powder nozzle exit for the laser beam and the shield gas.

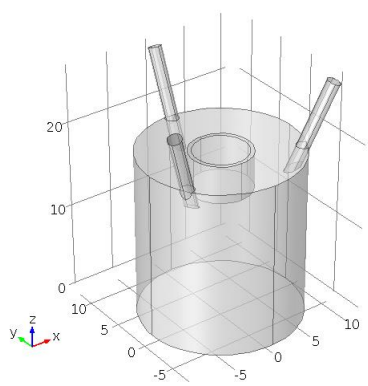

Fig. 3. Model geometry

Inside the model domain the Navier-Stokes equations

$$\rho(\mathbf{u}\cdot\nabla)\mathbf{u}=\nabla\left[-p\mathbf{I}+(\mu+\mu_t)\left(\nabla\mathbf{u}+(\nabla\mathbf{u})^T\right)\right]+\mathbf{F} \quad (1)$$

$$\rho\nabla\cdot\mathbf{u}=0 \quad (2)$$

with the density ρ, fluid velocity **u**, pressure p, unity tensor **I**, dynamic viscosity μ and any volume force **F** are solved. The eddy viscosity

$$\mu_t=\rho C_\mu\frac{k^2}{\varepsilon} \quad (3)$$

according to Wilcox, 1998 is defined by the turbulent kinetic energy k and the turbulent dissipation rate ϵ, which can be obtained from the following equations:

$$\rho(\mathbf{u}\cdot\nabla)k=\nabla\cdot\left[\left(\mu+\frac{\mu_t}{\sigma_k}\right)\nabla k\right]+P_k-\rho\varepsilon \quad (4)$$

$$\rho(\mathbf{u}\cdot\nabla)\varepsilon=\nabla\cdot\left[\left(\mu+\frac{\mu_t}{\sigma_\varepsilon}\right)\nabla\varepsilon\right]+C_{\varepsilon1}\frac{\varepsilon}{k}P_k-C_{\varepsilon2}\rho\frac{\varepsilon^2}{k} \quad (5)$$

The turbulence model parameters C_μ, $C_{\epsilon1}$, $C_{\epsilon2}$, σ_k and σ_ϵ are given in Table 1, while Wilcox, 1998 indicates the Reynolds stress

$$P_k=\mu_t\left[\nabla\mathbf{u}:\left(\nabla\mathbf{u}+(\nabla\mathbf{u})^T\right)\right] \quad (6)$$

The flow close to solid walls is approximated by the wall functions, which are explained by Kuzmin et al., 2007 and Grotjans & Menter, 1998.
The most important boundary conditions are given by the carrier gas flow $\dot{V}_c$ and shield gas flow $\dot{V}_s$, which determine the fluid velocity at the carrier gas and powder inlet

$$u_c=\frac{\dot{V}_c}{A_c} \quad (7)$$

as well as the fluid velocity at the shield gas inlet

$$u_s=\frac{\dot{V}_s}{A_s} \quad (8)$$

with the carrier gas inlet cross-sectional area A_c or rather the shield gas inlet cross-sectional area A_s. These are determined by the powder channel diameter of 1.5 mm and the nozzle exit for the shield gas of 7.0 mm

in diameter.

Table 1. Turbulence model parameters

$C_{\epsilon 1}$	$C_{\epsilon 2}$	C_{μ}	σ_{ϵ}	σ_k
1.44	1.92	0.09	1.3	1

After the fluid dynamics simulation the powder particle movement is calculated from Newton's second law

$$\frac{d\left(m_p \mathbf{v}\right)}{dt} = \mathbf{F_{drag}} + \mathbf{F_g} \tag{9}$$

with the particle mass m_p, particle velocity $\mathbf{v}$, gravity force $\mathbf{F_g}$ and drag force

$$\mathbf{F_{drag}} = \frac{3\mu \cdot 24\left[1 + 0.15\left(\frac{\rho \|\mathbf{u}-\mathbf{v}\| d_p}{\mu}\right)^{0.687}\right]}{4\rho_p \cdot d_p^2} \cdot m_p\left(\mathbf{u} + \zeta\sqrt{\frac{2k}{3}} - \mathbf{v}\right) \tag{10}$$

which is explained by Ochieng & Onyango, 2008 following the Schiller-Naumann drag law. Here d_p is the particle diameter, ρ_p the particle density and ζ a standard distributed random number with zero mean and unit standard deviation. So the term $\zeta\sqrt{2k/3}$ takes the influence of the turbulent flow on the particles into account. If a particle hits a powder nozzle wall at the initial velocity $\mathbf{v_c}$, the bounce condition defines the velocity

$$\mathbf{v} = \mathbf{v_c} - 2\left(\mathbf{n} \cdot \mathbf{v_c}\right)\mathbf{n} \tag{11}$$

after reflection with the normal vector $\mathbf{n}$ of the wall surface. At the carrier gas and powder inlet the initial particle velocity

$$\mathbf{v}_0 = -0.45 \cdot u_c \cdot \mathbf{n} + 0.036 \cdot u_c \cdot \begin{pmatrix} \zeta_1 \\ \zeta_2 \\ 0 \end{pmatrix} \tag{12}$$

is determined by the velocity at the carrier gas and powder inlet u_c. This is because measurements based on high speed camera videos showed, that the particle velocity at the nozzle exit is always $0.45 \cdot u_c$ both for a carrier gas flow $\dot{V}_c$=3.5 l/min as well as $\dot{V}_c$=5.0 l/min regardless of the powder feed rate at least in the range from 7.5 g/min up to 33.6 g/min. Additionally, the second term on the right of equation (12) gives the powder jet a divergence angle through the random numbers ζ_1 and ζ_2, so that the powder jet diameter in the working plane corresponds with the measurements results. The measurement data points from Fig. 2 (right) are plotted again in Fig. 4, which shows that that the measurement data points and the simulation

data points are distributed approximately with axial symmetry around the center axis of the powder nozzle, so that the powder particle density distribution m_t can be represented by a fit curve, which solely depends on the radius r instead of the coordinates x and y. The powder particle density distribution m_t is standardized, so that the volume below the rotationally symmetrical 3D surface equals 1. See Fig. 2 (right). The pattern of the measurement data points can be explained by the backlash of the machine axes as each circular path can be identified as a group of measurement data points, which lie on a curve deviating from the fit curve with a repeating shape. The simulation data points can be fitted by

$$m_t = 107045 \cdot e^{-\left(\frac{r+0.00018688\,\mathrm{m}}{0.0018878\,\mathrm{m}}\right)^2} \qquad (13)$$

and agree with the measurement data.

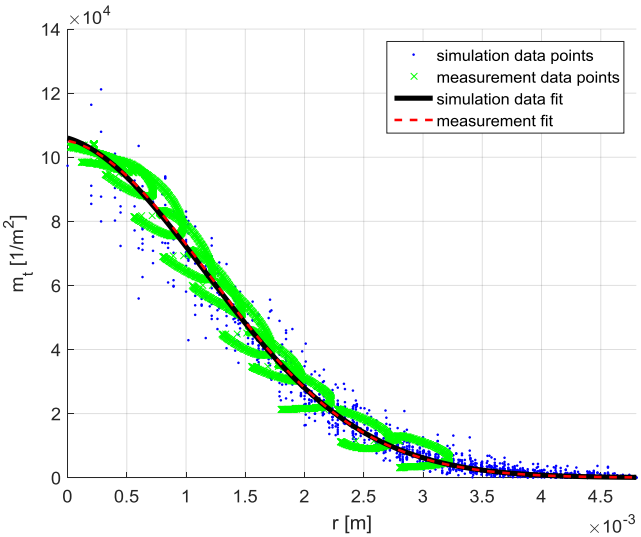

Fig. 4. Powder particle density distribution in simulation and measurement (MetcoClad® 625, powder feed rate 30 g/min, $\dot{V}_s$=$\dot{V}_c$=5 l/min)

So the simulation model results can be used to calculate the local attenuation percentage of the laser beam by the flying powder particles on the melt pool surface shown in Fig. 5 (left), where the attenuation was calculated within a radius of 5 mm around the beam axis assuming a negligible laser beam divergence angle. In contrast to the powder particle density distribution the attenuation is not rotationally symmetric, because the powder particle density distribution only becomes axisymmetric in the working plane when the powder jets from the three powder channels of the powder nozzle merge. But the results show, that the attenuation is negligible under the given conditions. Its effect on the shape of a laser beam with Gaussian intensity distribution can only clearly be seen for a large laser beam diameter of 6 mm, when the attenuation is multiplied by a factor of 4.3, so exaggerated conditions, which may be achieved by a higher powder feed rate and lower carrier gas flow. This situation is shown in Fig. 5 (right), where the intensity of laser radiation in the working plane is plotted. Here it is not considered, that the attenuated laser radiation may be absorbed by the flying powder particles, which contribute to the energy balance of the melt pool.

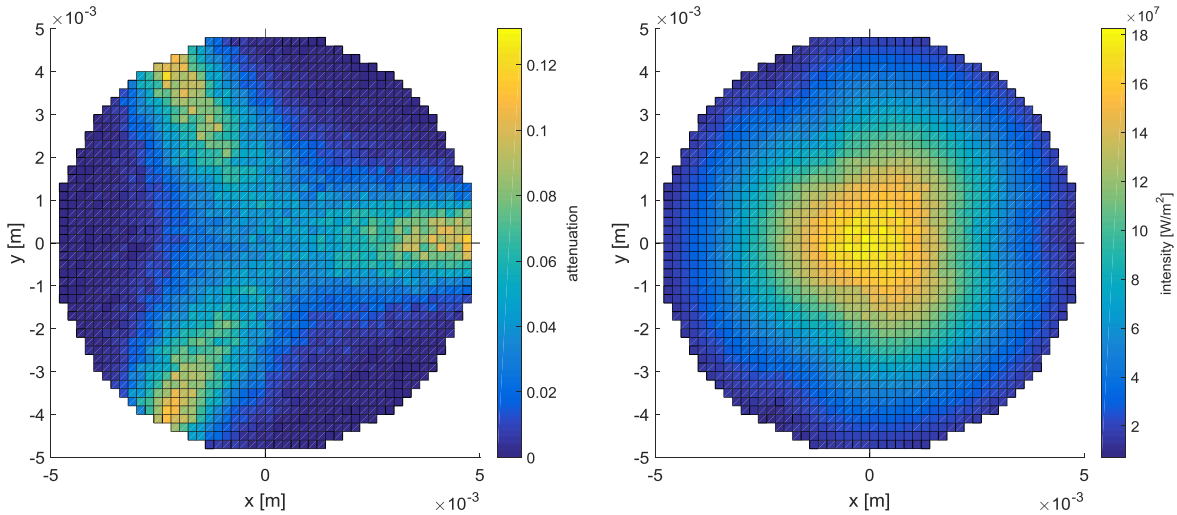

Fig. 5. Powder attenuation (left, MetcoClad® 625, powder feed rate 30 g/min, $\dot{V}_s$=$\dot{V}_c$=5 l/min) and the effect of attenuation on the resulting intensity on the workpiece surface (right)

3. Powder particle absorptivity measurement

After correct simulation of the powder jet a reliable prediction of the powder particle temperature is only possible when the absorptivity of the separate powder particles is known. The absorptivity of powder materials in form of a powder bed has already been measured by Tolochko et al., 2000 and others. In their measurement setup a closed thick powder layer is irradiated by a laser beam, while the reflected radiation is measured by an integrating sphere. There takes place however multiple reflection and absorption inside the powder bed, so that the measured absorptivity is higher than that of separated powder particles as they are in the powder jet. Rubenchik et al., 2015 carried out a caloric measurement, where an isolated powder bed is irradiated and the equilibrium temperature is measured. Here again multiple reflection and absorption interfere. Picasso et al., 1994 estimated the powder particle absorptivity from the laser particle interaction time in conjunction with the laser power, which is required to make the particles glow when passing the laser beam. The combination of absorptivity and attenuation measurement presented by Wirth et al., 2016 only gives an estimate for the powder absorptivity. As the commonly used ellipsometry measurement method can only be applied for flat surfaces, a new measurement method had to be developed in order to obtain accurate results. Fig. 6 shows the three most promising elaborated measurement concepts.

In all cases a power meter captures the laser power transmitted through the powder cloud, hence the fraction of laser power of the radiation interacting with the powder particles is known as there is no workpiece or melt pool surface in between. In the first concept, a powder jet crosses the laser beam and the average temperature of the powder particles is measured. Experiments showed however that the particle speed has to be low and the fraction of powder inside the stream high enough to ensure the particles do not cool down before reaching the temperature measurement device. This in turn leads to the need for a dense powder cloud with multiple reflection and absorption, so that the measured absorptivity depends on the powder feed rate. In the second concept, the homogeneously distributed powder particles are embedded in a transparent material and after a defined exposure time the absorbed energy is determined by putting the sample into a calorimeter. The sample is produced by mixing powder particles with a highly viscous polymer, which is subsequently cured. Here the low thermal conductivity of the polymer might cause problems like

temporary excessive local heating around powder particles or too long periods of time for temperature homogenization inside the calorimeter. The third concept tries to circumvent these problems. Here the laser beam passes an integrating sphere, which captures the power of the radiation reflected by the powder particles embedded in a transparent material.

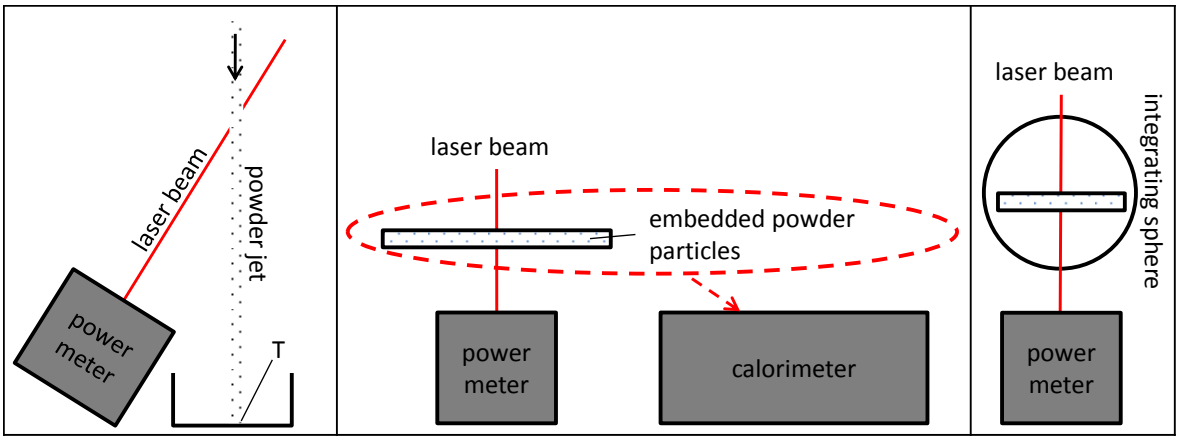

Fig. 6. Powder particle absorptivity measurement concepts

4. Conclusion and outlook

The powder particle density distribution in the working plane can be measured with little effort using a continuously recording balance. This allows the characterization of powder nozzles, for example in judging the state of wear or in order to obtain the powder particle density distribution as input data for melt pool process simulation.

The presented powder jet simulation model builds on the powder particle density distribution measurement results in the working plane and on particle velocity measurement at the powder nozzle exit, so that it realistically reflects the powder jet behavior in between. Subsequently, the interaction between flying powder particles and laser beam can be investigated by simulation. Consequently, further input data for melt pool process simulation may be derived such as attenuation values and the process may be optimized for instance regarding powder particle temperatures in high-speed laser cladding. Of course, for the latter purpose, another powder nozzle than the one analyzed herein has to be considered, which shows little interaction between powder particles and laser beam.

The previously mentioned powder particle temperature calculation requires additionally powder particle absorptivity data. Up to now no powder particle absorptivity measurement method can be found in literature, which reveals the absorptivity of separated powder particles as opposed to that of a powder bed. While a first measurement concept failed, two more ideas are herein presented and will be tested.

Acknowledgements

The authors wish to acknowledge the financial support granted by the Swiss Commission for Technology and Innovation (CTI) under grant number 19177.2 as well as the support and advice of the industrial partner Oerlikon Metco, particularly Dr. Arkadi Zikin and Jörg Spatzier.

References

Grotjans, H., Menter, F. R., 1998. Wall Functions for General Application CFD Codes. ECCOMAS 98, Proceedings of the Fourth European Computational Fluid Dynamics Conference, John Wiley & Sons, pp. 1112–1117.

Huang, Y. L., Liu, J., Ma, N. H., Li, J. G., 2006. Three-dimensional analytical model on laser-powder interaction during laser cladding. Journal of Laser Applications 18 (1), pp. 42-46.

Ibarra-Medina, J., Vogel, M., Pinkerton, A. J., 2011. A CFD model of laser cladding: from deposition head to melt pool dynamics. Proc. ICALEO'2011, pp. 23-27.

Kuzmin, D., Mierka, O., Turek, S., 2007. On the implementation of the κ-ε turbulence model in incompressible flow solvers based on a finite element discretisation. International Journal of Computing Science and Mathematics 1 (2-4), pp. 193-206.

Marsden, C. F., Frenk, A., Wagnière, J.-D., 1992. Power absorption during the laser cladding process, in: "Proc. of the European Conference on Laser Treatment of Materials 1992, Göttingen (ECLAT '92)". In: Mordike B. L.; Bergmann, H. W. (Eds.). DGM Oberursel, pp. 375-380.

Melo, L. D., 2015. Powder jet particle density distribution analysis and qualification for the laser metal deposition process. Dissertation Universidade Federal de Santa Catarina.

Morville, S., Carin, M., Carron, D., Le Masson, P., Gharbi, M., Peyre, P., Fabbro, R., 2012. Numerical Modeling of Powder Flow During Coaxial Laser Direct Metal Deposition-Comparison Between Ti-6Al-4V Alloy and Stainless Steel 316L, in Proceedings of the 2012 COMSOL Conference, Milan.

Mueller, M., Hentschel, O., Schmidt, M., Franke, J., 2016. Copper circuit traces by laser cladding with powder injection for additive manufactured mechatronic devices. 2016 IEEE 18th Electronics Packaging Technology Conference (EPTC), pp. 602-605.

Ochieng, A., Onyango, M. S., 2008. Drag models, solids concentration and velocity distribution in a stirred tank. Powder Technology 181 (1), pp. 1-8.

Picasso, M., Marsden, C. F., Wagniere, J. D., Frenk, A., Rappaz, M., 1994. A simple but realistic model for laser cladding. Metallurgical and Materials Transactions B 25(2), pp. 281-291.

Pinkerton, A. J., 2007. An analytical model of beam attenuation and powder heating during coaxial laser direct metal deposition. Journal of Physics D: Applied Physics 40(23), pp. 7323-7334.

Rubenchik, A., Wu, S., Mitchell, S., Golosker, I., LeBlanc, M., Peterson, N., 2015. Direct measurements of temperature-dependent laser absorptivity of metal powders. Applied optics 54(24), pp. 7230-7233.

Schopphoven, T., Gasser, A., Wissenbach, K., Poprawe, R., 2016. Investigations on ultra-high-speed laser material deposition as alternative for hard chrome plating and thermal spraying. Journal of Laser Applications 28(2), 022501.

Tabernero, I., Lamikiz, A., Martinez, S., Ukar, E., De Lacalle, L. L., 2012. Modelling of energy attenuation due to powder flow-laser beam interaction during laser cladding process. Journal of Materials Processing Technology 212(2), pp. 516-522.

Tolochko, N. K., Khlopkov, Y. V., Mozzharov, S. E., Ignatiev, M. B., Laoui, T., Titov, V. I., 2000. Absorptance of powder materials suitable for laser sintering. Rapid Prototyping Journal 6(3), pp. 155-161.

Weisheit, A., Gasser, A., Backes, G., Jambor, T., Pirch, N., Wissenbach, K., 2013. Direct Laser Cladding, Current Status and Future Scope of Application, in "Laser-Assisted Fabrication of Materials". In: Majumdar, J. D., Manna, I. (Eds.). Springer Heidelberg New York Dordrecht London, pp. 221-240.

Wilcox, D. C., 1998. Turbulence modeling for CFD, 2nd ed., DWC Industries.

Wirth, F., Eisenbarth, D., Wegener, K., 2016. Absorptivity measurements and heat source modeling to simulate laser cladding. Physics Procedia 83, pp. 1424-1434.

Zhang, B., Coddet, C., 2016. Numerical study on the effect of pressure and nozzle dimension on particle distribution and velocity in laser cladding under vacuum base on CFD. Journal of Manufacturing Processes 23, pp. 54-60.

Zekovic, S., Dwivedi, R., Kovacevic, R., 2007. Numerical simulation and experimental investigation of gas–powder flow from radially symmetrical nozzles in laser-based direct metal deposition. International Journal of Machine Tools and Manufacture 47(1), pp. 112-123.